

A NOVEL APPROACH TO PREDICTING THE CUTTING FORCE IN TURNING USING DIMENSIONAL ANALYSIS

Jelena Stanojković¹, Miloš Madić², Milan Trifunović²,
Predrag Janković², Dušan Petković²

¹University of Priština, Faculty of Technical Sciences, Serbia

²University of Niš, Faculty of Mechanical Engineering in Niš, Serbia

Abstract. *Cutting forces are a critical indicator of the machining process, and their modeling is important for a variety of reasons, including tool life assessment, chatter prediction, tool condition monitoring, assessment of machining strategies and machining process optimization and control. This paper presents a new principle of modeling the main cutting force using dimensional analysis (DA). Dry longitudinal single-pass turning of two different steels (20MnCrS5 and S235JRG2) with two different cutting inserts, was considered. Taguchi's $3^3 \times 2^1$ design with 6 trials was applied to arrange seven parameters: depth of cut, feed rate, cutting speed, feed velocity, rake angle, cutting edge angle, and workpiece material parameter, i.e., tensile strength. The obtained results, including additional validation tests, showed a very good prediction capacity of the DA-based model in estimating the cutting force during the turning process. The analysis includes the influence of parameters on the cutting force as well as examination of 3D surface diagrams and correlation coefficients. The chip slenderness ratio proved to be the most important dimensionless group for cutting force prediction. By performing additional experimental trials, the correction coefficient for the tool nose radius was estimated and extended models were developed. The well-known Victor-Kienzle model can be used to predict the cutting force if the exact values of m_c and $k_{c1.1}$ coefficients. The proposed DA-based models proved to be valid for predicting all three cutting force components with high accuracy.*

Key words: *Turning, Cutting force, Dimensional Analysis, Modeling, Taguchi's Design*

Received: November 29, 2024 / Accepted March 01, 2025

Corresponding author: Jelena Stanojković

Faculty of Technical Sciences, University of Priština in Kosovska Mitrovica, Knjaza Miloša 7, 38220 Kosovska Mitrovica, Serbia

E-mail: jelena.stanojkovic@pr.ac.rs

1. INTRODUCTION

The turning process is one of the most commonly used in the metal processing industry's production operations [1]. As one of the oldest production technologies, it still plays an important role in modern industry due to favorable cutting mechanics for a wide range of materials, and can ensure high productivity at acceptable costs [2]. Nonetheless, as well as other traditional and non-traditional technologies [3-5], turning is a multi-input process characterized by the existence of multiple machinability and output performances. In addition, these performances for a particular application can be of different significance, and as a rule, are mutually opposed [5].

Cutting forces are one of the most important machinability indicators for understanding the turning process. The cutting forces generated during the turning process have a direct impact on heat generation, which in turn affects tool life and machining accuracy. They also correlate with other factors, such as the quality of the machined surface, self-excitation, and forced vibrations [6-8]. Knowing the cutting forces for different cutting parameters helps the designer-manufacturer increase the machine tool's efficiency. In addition, it enables the optimization of processing parameters, which can lead to improved productivity, reduced production costs, and increased process efficiency [9-11].

In order to achieve a complete match between the predicted and real responses, it is necessary to capture all aspects of the interactions of the cutting tool, workpiece, machine tool, and environment. However, in practice, this is often difficult because the actual states of some aspects and physical phenomena are unknown or partially known in a given process or even certain parameter space. These aspects also include environmental influences, homogeneity of the workpiece material chemical composition and mechanical properties, variable lubrication and chip removal conditions, random formation of deposits and their removal, etc. [12]. Therefore, general modeling approaches are based on simplifying the real process.

Various influencing factors, including processing parameters, workpiece material properties, the kinematics and dynamics of the cutting process, cutting tool geometry, and lubrication conditions, have led to the establishment of numerous cutting force prediction models today. Various methods exist for modeling the cutting force, typically categorized as analytical, empirical, and numerical methods [13]. In practice, empirical models, with the Victor-Kienzle model being one of the most frequently applied approaches, are used in determining cutting forces [14].

Empirical models are based on experimental determination of the model coefficients, whose form has been usually determined in advance, and typically relate cutting force as the dependent variable to different independent variables such as cutting speed, depth of cut, feed rate, material type, cutting tool geometry, etc. These empirical models are often simple to implement and provide acceptable results in a wide range of industrial applications.

Different researchers have previously used different approaches to predict the cutting force during the turning process, Table 1.

Table 1 Review prediction of the cutting force during the turning process

Ref.	Tool	Material workpiece	Process parameters	Experimental design (trials)	Model type
[15]	coated carbide	AISI 4340 steel	v_c, f, a_p	Taguchi (27)	linear
[16]	ceramic with reference	AISI D3 steel	v_c, f, a_p, CT	Taguchi (18)	quasi-linear ANN
[17]	coated carbide	36CrNiMo4 alloy steel	f, a_p, r_e	Taguchi (9)	linear
[18]	cubic boron nitride	AISI H11 steel	v_c, f, a_p, H	Box-Behnken (29)	quadratic nonlinear model with interactions
[19]	mixed ceramic	AISI 4140 steel	v_c, f, a_p, r_e	Box-Behnken (29)	quadratic nonlinear ANN
[20]	polycrystalline cubic boron nitride	AISI D2 steel	v_c, f, a_p, H, r_e	Taguchi (27)	quasi-linear power
[21]	cubic boron nitride 7020	AISI 52100 steel	v_c, f, a_p, H	FFD (25)	ANN
[22]	tungsten-coated carbide	AISI 4340 alloy steel	v_c, f, a_p, r_e	FFD (60)	GPR SVM ANN
[23]	multi-layer coated carbide	D3 steel	v_c, f, a_p, r_e	Taguchi (16)	linear ANN
[24]	PVD micro grain	Inconel 718	v_c, f, a_p, h	Taguchi (27)	mechanistic
[25]	TiAlN coated carbide	AISI 420 steel	v_c, f	FD with two central points (11)	quadratic

FFD (Full Factorial Design), FD (Factorial Design), ANN (Artificial Neural Network), GRP (Gaussian Process Regression), SVM (Support Vector Machines), GP (Genetic Programming), v_c (cutting speed) m/min, f (feed rate) mm/rev, a_p (depth of cut) mm, CT (cutting tool), H (workpiece hardness) HRC, h (chip thickness) mm.

Krupa et al. [26] developed a mathematical model and proposed a method for estimating the feed rate impact of stochasticity on the main cutting force in turning. They performed measurements of the main cutting force during turning on universal lathes, with the 45 steel (ISO P) (carbon content 0.45%) workpiece material, a T15K6 cutting tool without coating, and feed rate values of 0.06, 0.1, 0.15 and 0.2 mm/rev. The mathematical model was developed, and dispersion characteristics (mean value, dispersion, and mean square deviation) of the main cutting force were obtained, depending on the corresponding dispersion characteristics of feed rate. Fodor et al. [27] introduced a stochastic extension of the existing cutting force models. They showed that the cutting force is stochastic with a variance of the measured cutting force of around 4-9% of the average value, depending on the selected parameters. Abdellaoui et al. [28] investigated the effects of tool nose radius in the turning process. They developed a thermomechanical model related to the average

tool/chip contact temperature, which enabled the prediction of all thermomechanical parameters when cutting with a sharp tool. As a function of the value of the minimum uncut chip thickness, two cutting situations were defined (plowing and cutting). Horvath [29] presented a review of the main research results of recent years regarding the cutting force, where the cutting forces in turning depend not only on the material properties and cutting parameters, but also to a large extent on the geometry of the tool edge that determines the shape of the chip (thickness and width). He derived a new cutting force model for fine turning, which can be used to estimate the main cutting force.

It can be observed from the literature review that the researchers used different methods to derive cutting force prediction models. Each method makes the prediction fairly accurate, but it comes with limitations such as needing to do more experimental trials, finding the best form of the model, optimizing hyper-parameters, overfitting, and so on, which makes it not so receptive to developing and applying in real production conditions. Therefore, the primary goal of this study is to propose a new cutting force prediction model, developable with a limited number of experimental trials while taking into account different parameters that influence the turning process such as the workpiece and the cutting tool properties as well as main cutting parameters. The approach is based on the principles of dimensional analysis (DA), and in this study these models were developed for the prediction of cutting forces in dry single-pass medium turning of two steels, 20MnCrS5 and S235JRG2. To this aim, Taguchi's orthogonal experimental design with six trials was used for the arrangement of three dimensionless groups while considering seven input process parameters. Four of them are related to the machining process (depth of cut, feed rate, feed velocity, and cutting speed), two are related to the geometry of the cutting tool (cutting edge angle and rake angle), and one is the workpiece material parameter (tensile strength). The obtained experimental results of the main cutting force were compared with the predicted values to determine the percentage error. The percentage error of additional validation tests was further estimated while using parameter values outside the initial experimental hyperspace. The analysis of the obtained results included which parameter, i.e., dimensionless group, had the greatest influence on the cutting force, as well as determining the correlation coefficients. The percentage error of the experimental and validation tests of the Victor-Kienzle model of the main cutting force was determined with the coefficients ($m_c, k_{c1,1}$) taken from the literature. An extended model of the main cutting force depending on one more cutting parameter, i.e., tool nose radius, was also proposed. Finally, the mutual dependences of all three components of the cutting force were analyzed with respect to the identified dimensionless group with the greatest influence.

2. DIMENSIONAL ANALYSIS OF THE CUTTING FORCE

In physics and engineering, many parameters and measurements take the form of numerical quantities with corresponding dimensional units [30]. DA is a powerful tool that aids in the design, ordering, performance, analysis, and synthesis of the resulting data [31]. In general, it is a mathematical tool used to simplify a problem by reducing the number of variables to the smallest number of essential parameters and a technique that enables the conversion of physical quantities from one unit of measurement to another, and the conversion of the basic physical quantities of the SI system of measurements with their dimensions (length- L , time- T , mass- M , thermodynamic temperature- θ , electric current- I ,

luminous intensity- J , amount of substance- N) [32]. Parameters are described by dimensionless groups (π groups) that connect independent variables with dependent variables. The primary benefit of this method is its significant reduction in the number of experimental trials needed to determine the relationship between variables, thereby reducing both costs and development time. This study uses the Buckingham π -theorem as the main tool for the reduction of variables.

The Buckingham π -theorem, as a key concept of DA, helps simplify complex physical problems by reducing the number of variables involved. It is necessary to select the repeating and non-repeating variables for model development [33]. According to the Buckingham π -theorem, “the number of independent dimensionless groups that may be employed to describe a phenomenon known to involve n variables is equal to the number $n-m$, where m is usually the number of basic dimensions needed to express the variables dimensionally” [33]. It is necessary to fulfill two basic criteria before using DA [34]:

- principle of dimensional homogeneity, and
- all relevant variables are included in the proposed relationship.

The principle of dimensional homogeneity is based on the fact that in order to establish equality, the dimensions and units in each term of an equation must be the same. The equation is dimensionally homogeneous if this condition is satisfied DA [33].

In the present study, DA was used to derive a model for predicting the cutting force in turning, initially for predicting the main cutting force (F_c), Figure 1.

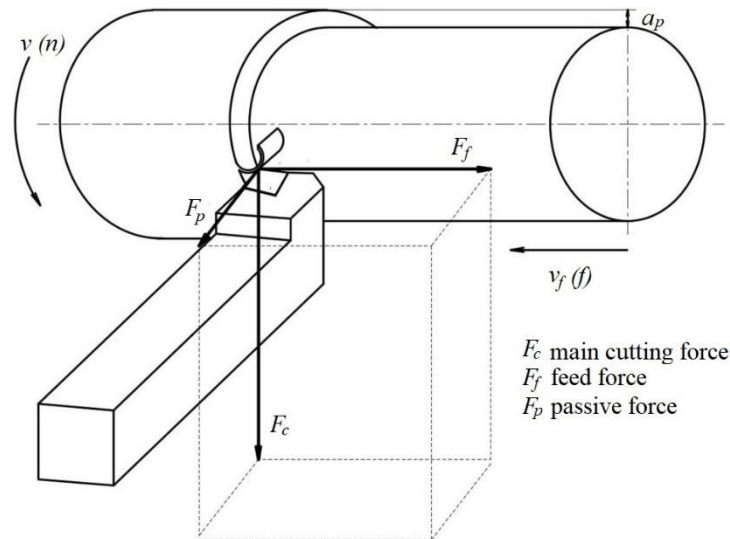


Fig. 1 Cutting force components in turning

The dimensions of the cutting force and the parameters that are defined based on the basic dimensions, i.e. length (L), time (T), mass (M), which affect the main cutting force, are as follows:

- Main cutting force (F_c): MLT^{-2}
- Tensile strength (R_m): $ML^{-1}T^{-2}$

- Feed rate (f): L
- Cutting speed (v): LT^{-1}
- Feed velocity (v_f): LT^{-1}
- Depth of cut (a_p): L
- Rake angle (γ_0): –
- Cutting edge angle (κ): –

Rake angle and cutting edge angle have no dimensions. The dependent parameter is the main cutting force, and the independent parameters are tensile strength, depth of cut, cutting speed, feed rate, feed velocity, rake angle and cutting edge angle. Feed velocity, feed rate, and rake angle were selected as repeating parameters. By applying Buckingham π -theorem, the π_1 group can be represented by the following form:

$$\pi_1 = F_c \cdot R_m^a \cdot v_f^b \cdot f^c \cdot \gamma_0^d \quad (1)$$

By changing the dimensions, equation 1 has the following form:

$$\pi_1 = (MLT^{-2}) \cdot (ML^{-1}T^{-2})^a \cdot (LT^{-1})^b \cdot (L)^c \quad (2)$$

Only those values with the same dimension are added. Addition by MLT is shown in the following forms:

$$M : 1 + a = 0 \quad (3)$$

$$L : 1 - a + b + c = 0 \quad (4)$$

$$T : -2 - 2 \cdot a - b = 0 \quad (5)$$

By solving the system of three equations with three variables, the values of the unknowns are obtained: $a=-1$, $b=0$ and $c=-2$. Based on the obtained values for each dimension in the initial π_1 group, equation (1), the is replaced with the obtained values and the value of the π_1 group can be represented by the following form:

$$\pi_1 = F_c \cdot R_m^{-1} \cdot f^{-2} = \frac{F_c}{R_m \cdot f^2} \quad (6)$$

In this case, there are four dimensionless groups, π_1 , π_2 , π_3 , π_4 , other π groups are obtained in the same way and presented in Table 2.

Table 2 Four dimensionless (π) groups

π_1	π_2	π_3	π_4
$\frac{F_c}{R_m \cdot f^2}$	$\frac{v}{v_f}$	$\frac{a_p}{f}$	$\frac{\kappa}{\gamma_0}$

If one sets: $\pi_1=f(\pi_2, \pi_3, \pi_4)$, the main cutting force as the function of dimensionless groups can be represented by the following model:

$$F_c = x_1 \cdot R_m \cdot f^2 \cdot \left(\frac{v}{v_f}\right)^{x_2} \cdot \left(\frac{a_p}{f}\right)^{x_3} \cdot \left(\frac{\kappa}{\gamma_0}\right)^{x_4} \quad (7)$$

3. EXPERIMENTAL SETUP

The experiments of dry longitudinal single-pass turning were performed on a “POTISJE” PA-C 30 universal lathe, with the power of 11 kW, spindle speed range of 20÷2000 rpm, and longitudinal feed rate range of 0.04÷9.136 mm/rev, in laboratory conditions. The cutting tool was Sandvik Coromant PCLNR 3225P 12 tool holder (cutting edge angle of $\kappa=95^\circ$, rake angle of $\gamma_{oh}=-6^\circ$) with cutting inserts CNMG 120408E-SF ($\gamma_{oi}=14.5^\circ$, tool nose radius of $r_e=0.8\text{mm}$) and CNMG 120408E-NF ($\gamma_{oi}=25^\circ$, tool nose radius of $r_e=0.8\text{mm}$), manufactured by Dormer Pramet, of T8430 grade (PVD coated fine grained cemented carbide, suitable for higher feed rates and medium to lower cutting speeds). The workpiece materials used in this experiment were 20MnCrS5 and S235JRG2 steel. 20MnCrS5 is an alloy steel with excellent mechanical properties, which makes it suitable for a wide range of applications in various industries. Its strength, toughness, and wear resistance ensure the durability and reliability of components made of this material. It is most widely used in the automotive and mechanical industries (for the production of machine parts that suffer heavy loads and wear, including spindles, gears, and bearings). According to Dormer Pramet, it belongs to the workpiece material group P3.2 (alloy steels (carbon steels with an alloying content $\leq 10\%$) with a hardness of 180-260 HB). S235JRG2 is a carbon construction steel that has a specific application thanks to its mechanical properties and chemical composition. It is most widely used in the construction industry, infrastructure, mechanical engineering, etc. According to Dormer Pramet, it belongs to the workpiece material group P2.1 (plain carbon steels (steels comprised of mainly iron and carbon) containing $< 0.25\%$ C with a hardness of < 180 HB). Chemical composition of the workpiece materials 20MnCrS5 and S235JRG2 are shown in Table 3. The sample of cylindrical rods used in these experiments had different diameters (55 and 59 mm) and the same length of 250 mm.

Table 3 Chemical composition of the workpiece materials

		Chemical composition [%]							
	C	Mn	Si	P	S	Cr	Ni	Mo	Al
20MnCrS5	0.018	1.11	0.24	0.016	0.026	1.07	0.08	0.018	0.026
	Cu	As	V	Ti	B	N	Cev.	Ca	Sn
	0.19	0.007	0.007	0.024	0.0003	0.007	0.602	-	-
S235JRG2	C	Mn	Si	P	S	Cr	Ni	Mo	Al
	0.16	0.46	0.176	0.013	0.005	0.08	0.04	0.01	0.012
	Cu	As	V	Ti	B	N	Cev.	Ca	Sn
	0.08	0.03	<0.001	<0.001	0.0005	0.008	0.25	0.002	0.05

The HRB method was used to determine the hardness of workpiece materials. The hardness was measured on a Rockwell device scale B with standard indenter and test force. Tensile strength (R_m) was indirectly determined by using Conversion table A.1–

Standard ISO 18265:2003 Metallic materials–conversion of hardness values. For 20MnCrS5 hardness is 156 N/mm^2 and tensile strength is 525 N/mm^2 , while for S235JRG2 hardness is 163 N/mm^2 and tensile strength is 540 N/mm^2 .

Components of cutting force were measured using a three-component piezoelectrical force transducer, basic unit KISTLER Type 9265A and a tool holder KISTLER Type 9441, which was mounted on the lathe via a custom tool holder adapter creating a very rigid tooling fixture. The load signal is generated by the dynamometer and a Kistler type 5007 charge amplifier. Through the HBM QuantumX MX840 universal measuring amplifier–measuring data were acquired, visualized, and analyzed using the “Catman” data acquisition software.

The experimental setup included the machine tool, tool holder, cutting inserts, three-component dynamometer, charge amplifier, data acquisition unit, computer, software, input parameters, workpieces, and hardness measurement device. The experimental setup is shown in Fig. 2.

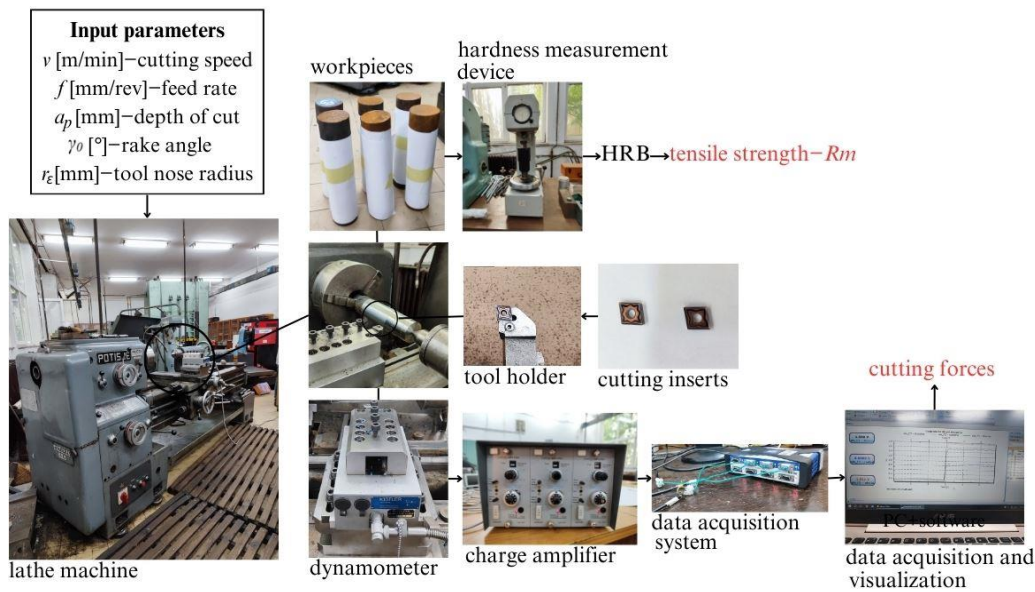


Fig. 2 Schematic representation of the experimental setup

The experiment was planned according to the form of the proposed main cutting force prediction model. In the study, seven parameters were considered, four related to the machining process (depth of cut, feed rate, feed velocity, and cutting speed), two related to the geometry of the cutting tool (cutting edge angle and rake angle), and one material parameter (tensile strength). Moreover, tool nose radius was also considered in additional experimental trials so as to determine the correction coefficient for the proposed cutting force prediction model.

Parameter ranges and levels were selected based on the tool manufacturer's recommended cutting conditions for the inserts. The experimental design used was the Taguchi orthogonal design (L_6) $3^3 \times 2^1$ [35]. Parameters with their names, symbols, units,

and values are shown in Table 4. The parameters were varied in accordance with the proposed main cutting force prediction model, i.e., defined by dimensionless π groups. Cutting speed and cutting edge angle for both experimental designs were taken as constant values because their influence on the main force is very small, almost negligible, as discussed by Stephenson and Agapiou [36], for most materials, except soft metals and temperature sensitive materials.

Table 4 Parameters with their names, symbols, units and values

Parameter	Symbol	Unit	20MnCrS5		S235JRG2	
			Values			
Cutting speed	v	m/min	157		245	
Feed rate	f	mm/rev	0.196	0.249	0.321	
Depth of cut	a_p	mm	1.2	1.8	1.9	2.0 2.9
Rake angle	γ_0	°		8.5	19	
Cutting edge angle	κ	°			95	
Tool nose radius	r_c	mm	0.8	1.2		

4. RESULTS AND DISCUSSION

4.1 DA Model of the Main Cutting Force

The main cutting force values obtained experimentally in laboratory conditions are shown in Tables 5 and 6 for 20MnCrS5 steel and S235JRG2 steel, respectively.

Based on the experimental data of the main cutting force and by minimizing the sum of squared errors using Matlab, the unknown coefficients of the proposed main cutting force prediction models were determined.

Main cutting force prediction models in dry longitudinal single-pass turning of two workpiece materials, 20MnCrS5 and S235JRG2 steels with a tool nose radius of 0.8 mm, were obtained in the following form:

$$(20\text{MnCrS5}) F_c = 2.4865 \cdot 525 \cdot f^2 \cdot \left(\frac{v}{v_f}\right)^{0.09816} \cdot \left(\frac{a_p}{f}\right)^{0.89362} \cdot \left(\frac{\kappa}{\gamma_0}\right)^{0.01669} \quad (8)$$

$$(S235JRG2) F_c = 1.4551 \cdot 540 \cdot f^2 \cdot \left(\frac{v}{v_f}\right)^{0.10746} \cdot \left(\frac{a_p}{f}\right)^{1.04605} \cdot \left(\frac{\kappa}{\gamma_0}\right)^{0.05254} \quad (9)$$

The predicted main cutting force values were compared with the main cutting force values obtained experimentally in order to determine the mean absolute percentage error (MAPE). The MAPE value of the DA model for steel 20MnCrS5 is about 0.38%, while for steel S235JRG2 is about 0.65%. Based on these results, it can be said that the developed main cutting force prediction models obtained by applying DA for both workpiece materials give quite good results from an engineering point of view.

Table 5 Experimental design $3^3 \times 2^1$ of the main cutting force of 20MnCrS5 steel

No.	A	B	C	v/v_f π_2	a_p/f π_3	κ/γ_o π_4	F_c [N] experimentally	F_c [N] DA model
1	0	0	-1	693.93	7.63	5.00	969	971.2
2	0	0	1	693.93	7.63	11.18	977	984.7
3	1	-1	-1	881.57	6.12	5.00	508	506.1
4	1	1	1	881.57	9.18	11.18	742	736.8
5	-1	1	-1	538.28	9.03	5.00	1831	1830.4
6	-1	-1	1	538.28	6.23	11.18	1334	1331.4

Table 6 Experimental design $3^3 \times 2^1$ of the main cutting force of S235JRG2 steel

No.	A	B	C	v/v_f π_2	a_p/f π_3	κ/γ_o π_4	F_c [N] experimentally	F_c [N] DA model
1	0	0	-1	744.39	7.63	5.00	895	904.1
2	0	0	1	744.39	7.63	11.18	939	943.1
3	1	-1	-1	945.68	6.12	5.00	465	456.5
4	1	1	1	945.68	9.18	11.18	731	727.8
5	-1	1	-1	577.43	9.03	5.00	1747	1744.5
6	-1	-1	1	577.43	6.23	11.18	1235	1233.7

With both steel materials, the influence of parameters A, B and C, i.e., the influence of dimensionless groups, π_2 , π_3 and π_4 , is quite the same for the main cutting force. Therefore, with an increase in the value of dimensionless groups, π_2 , π_3 and π_4 , the main cutting force increases, where the influence of a_p/f is dominant and the most pronounced, followed by groups π_4 and π_2 , for 20MnCrS5 steel, that is, groups π_2 and π_4 , for S235JRG2 steel.

Since the exponents of dimensionless groups are different, it is possible to see an increase in the main cutting force with an increase in the value of dimensionless group π_4 , i.e., a decrease in rake angle, more pronounced when turning S235JRG2 steel compared to 20MnCrS5 steel. The same applies to dimensionless group π_3 . Namely, the increase in the a_p/f ratio (chip slenderness ratio) rapidly increases the main cutting force when turning S235JRG2 steel compared to 20MnCrS5 steel.

Both investigated materials have approximately the same tensile strength (R_m), but the calculated coefficients of the DA model (C , x_1 , x_2 , x_3) are different, which indicates different machinability and the fact that one DA model cannot be used for accurate prediction of cutting force. If only one model was used, for example, the DA model of S235JRG2 steel for 20MnCrS5 steel, the MAPE for all experimental tests would be around 10%, and in the opposite case even 20%. The intercept values of derived models are significantly different (2.48 and 1.45) indicating that 20MnCrS5 steel is more difficult to machine compared to S235JRG2 steel.

Parameter A (dimensionless group π_2), i.e., the ratio of cutting speed and feed velocity, depends only on feed velocity because cutting speed was kept constant for given workpiece material in the experimentation. Feed velocity depends on feed rate and this ratio represents only the change in the feed rate value. This parameter has a positive correlation with the main cutting force, i.e., increasing parameter A increases the main cutting force. Too much increase can lead to machine tool overload and increased tool wear. In other words, a

decrease in feed rate results in a decrease in the main cutting force, since the cutting tool removes smaller layer of material. This implies that a smaller volume of material being removed requires less cutting force. Furthermore, removal of smaller volume of material results in reduction of the heat generated during cutting. The reduced temperature helps to maintain the mechanical properties of the cutting tool and material, which further reduces the main cutting force [37].

Parameter B (dimensionless group π_3), i.e., the ratio of depth of cut to feed rate, chip slenderness ratio, has a positive correlation with the main cutting force - by increasing the chip slenderness ratio the main cutting force increases sharply [37-39]. Increasing the cross-sectional area of the uncut chip and the volume of the deformed material, either by increasing depth of cut or feed rate, results in an increase in the main cutting force. Denkena et al. [40] have concluded the same about the influence of the undeformed cross-section of the chip and the volume of the deformed material on the main cutting force for alloy and carbon steel.

Parameter C (dimensionless group π_4), i.e., the ratio of the cutting edge angle and rake angle, also has a positive correlation with the main cutting force, but the effect is less pronounced. Thus, an increase in this parameter, which is accomplished by reducing rake angle, slightly increases the main cutting force. Increasing rake angle increases shear angle and results in a decrease in chip thickness, as well as a decrease in the main cutting force and therefore a decrease in cutting power [41]. Although large rake angles decrease the main cutting force, they simultaneously reduce the strength of the tool tip which ultimately may lead to its fracture.

The proposed main cutting force prediction models are visualized in Fig. 3. This figure shows 3D surface plots of the main cutting force (F_c) for both workpiece materials, 20MnCrS5 steel and S235JRG2 steel, depending on different dimensionless groups.

The diagrams clearly indicate that there are no interactions between dimensionless groups, i.e., there is no qualitative change in the influence of a certain dimensionless group in relation to another dimensionless groups. The absence of significant interactions of processing parameters (depth of cut, feed rate, cutting speed, feed velocity, rake angle, cutting edge angle) on the main cutting force was also previously reported [39]. The absence of significant interactions indicates the possibility of modeling input-output dependences with simpler models, which was done in this study by creating degree models using DA.

Adequate experimental validation of the proposed main cutting force prediction models is a necessary step to ensure that the models generalize well with new data, which is key to their application. Therefore, based on the perceived significance of dimensionless groups the additional cutting regimes were tested, Tables 6 and 7.

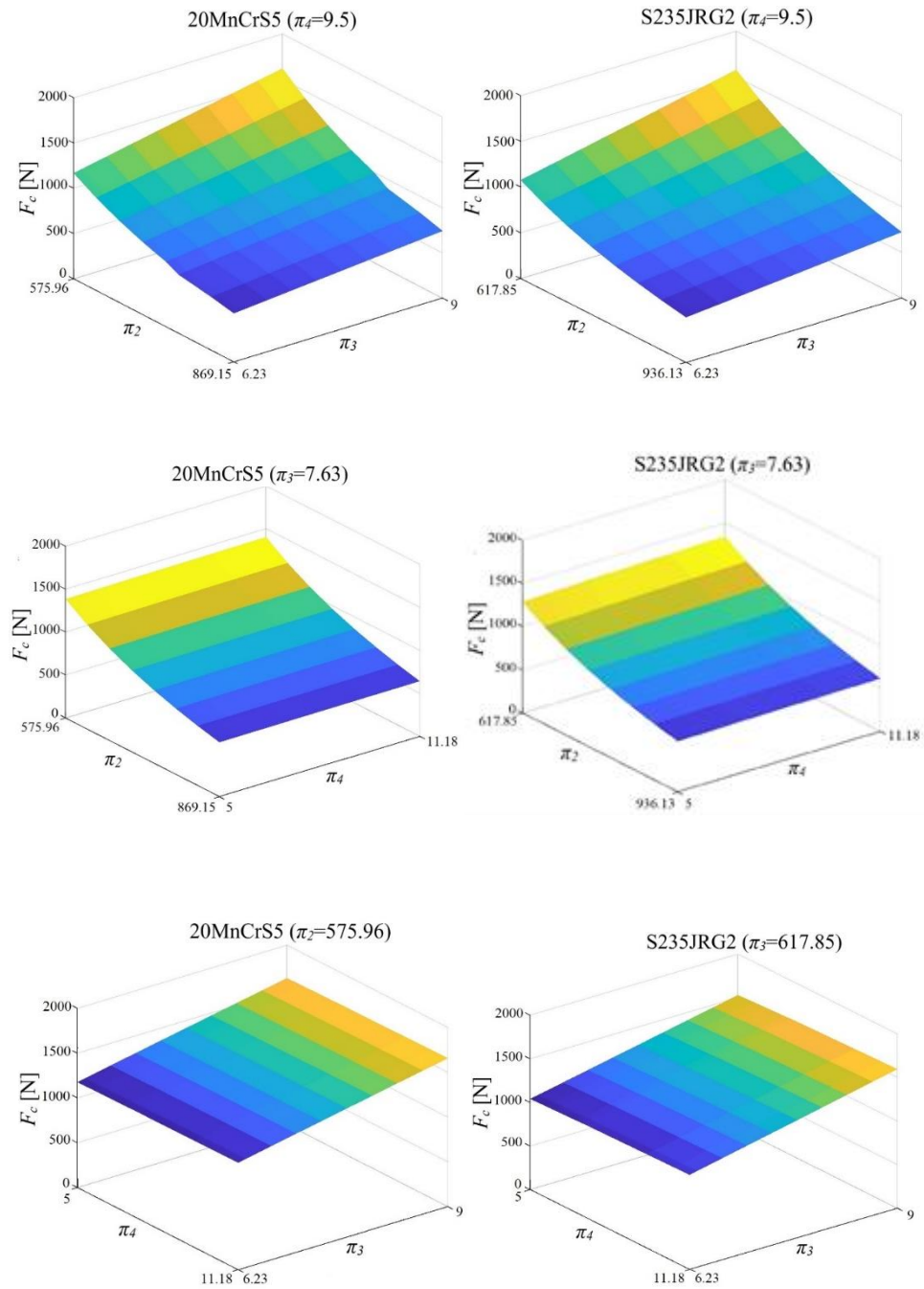


Fig. 3 Surface plot (3D plot) of the main cutting force (F_c) dependence on different π groups for 20MnCrS5 steel and S235JRG2 steel

The validation results for both materials show that predicted values are close to the experimentally obtained values. As can be seen from Tables 7 and 8, trials 3 and 4 are within the included experimental hyperspace, where the cutting force values obtained by the DA models are the closest to the values obtained experimentally.

Table 7 Main cutting force values for different validation cutting regimes (20MnCrS5)

No.	v/v_f π_2	a_p/f π_3	κ/γ_o π_4	F_c [N] experimentally	F_c [N] DA model
1	538.28	3.74	5.00	739	832.4
2	484.00	3.36	11.18	810	939.3
3	807.42	7.48	5.00	715	714.9
4	606.27	7.72	11.18	1248	1285.8
5	970.72	14.61	5.00	973	915.9
6	807.42	11.21	11.18	1069	1040.9

Table 8 Main cutting force values for different validation cutting regimes (235JRG2)

No.	v/v_f π_2	a_p/f π_3	κ/γ_o π_4	F_c [N] experimentally	F_c [N] DA model
1	577.43	3.74	5.00	735	693.1
2	519.20	3.36	11.18	794	791.1
3	866.14	7.48	5.00	658	664.4
4	650.36	7.72	11.18	1184	1232.5
5	1041.31	14.61	5.00	890	944.7
6	866.14	11.21	11.18	1005	1059.3

The MAPE for 20MnCrS5 steel is about 1.5% and for S235JRG2 steel is about 2.5%. The other cutting regimes are outside of the experimental hyperspace, in terms of the chosen parameter values. Taking into account the obtained results, the DA models give fairly satisfactory extrapolation results. For all validation tests, the MAPE for 20MnCrS5 steel is about 6.6%, which is borderline satisfactory from an engineering point of view. Results for S235JRG2 steel are much more favorable and amount to a MAPE value of about 3.78%.

Based on the obtained results, it can be concluded that the DA models provide the means to develop fairly accurate models for predicting the main cutting force during the turning process, using a small number of experimental trials, which result in the reduction of the cost of the experiment, savings in materials and energy, as well as reduced time

Prediction performances of the proposed DA models in the form of regression are given in Fig. 4. Values from the main experiment and additional validation trials were taken into consideration. The correlation coefficient for both workpiece materials is around 0.99, confirming the considerable accuracy of the developed DA models.

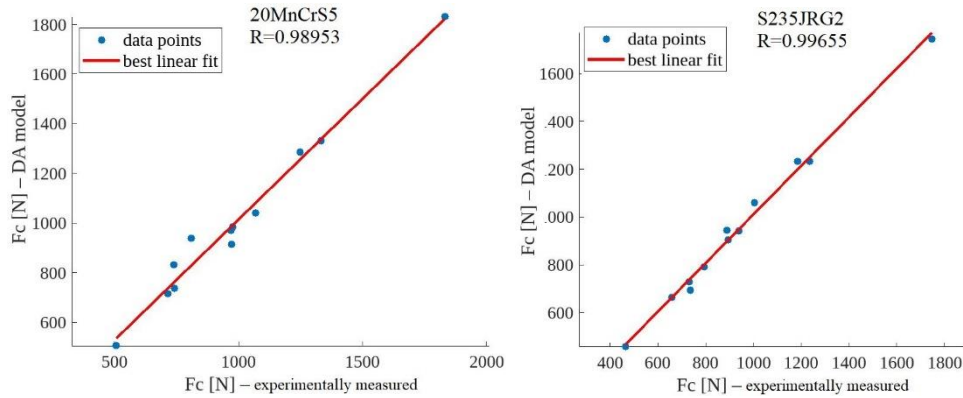


Fig. 4 Correlations between the predicted (DA model) and the experimentally measured values of the main cutting force using the entire data set

The proposed DA models were further verified using residual analysis. Figure 5 shows the residuals on the vertical axis and the values of the main cutting force for both steel materials (20MnCrS5 and S235JRG2) on the horizontal axis by considering experimental data from the main experiment and additional validation trials. The residuals do not follow any recognizable pattern and are scattered above and below zero.

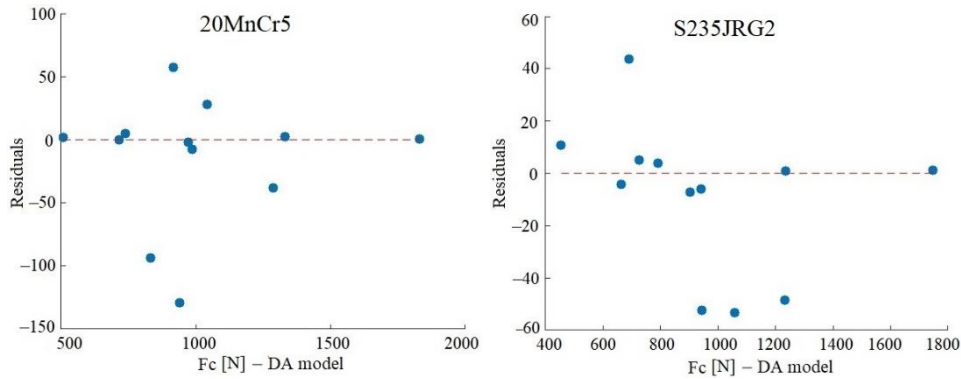


Fig. 5 Residual plot of the main cutting force

The models of the main cutting force for both steel materials yield good predictions in a wide range of chip slenderness ratio values, where significant changes in chip morphology occur. A higher chip slenderness ratio results in longer and thinner chips [42-44].

Figure 6 shows that the 20MnCrS5 steel chips are somewhat different, and more unfavorable as their form also depends on the mechanical properties such as hardness and microstructure of the material [45]. Materials with higher hardness have a lower ability to deform, so the chip breaks and is easily removed from the cutting zone, as is the case with 235JRG2 steel.



Fig. 6 Chip morphology as a function of chip slenderness ratio

Based on the initial experimental and validation tests, the main cutting force of 235JRG2 steel remains about 6% higher compared to 20MnCrS5 steel. However, when the values of a_p/f are less than 4, the main cutting forces are almost equal, which is not the case with the Victor-Kienzle model [46].

4.2 Victor-Kienzle Model of the Main Cutting Force

The well-known Victor-Kienzle model [15] is still widely used for the calculation of the main cutting force, which has the following form [46-48]:

$$F_c = A_1 \cdot k_{c1.1} \cdot h^{-m_c} \quad (10)$$

where A_1 (mm^2) is the cross-sectional area of the uncut chip, $k_{c1.1}$ (N/mm^2) is the specific cutting force for 1 mm^2 cross-sectional area of the cut, h (mm) is the uncut chip thickness, and m_c is the exponent of the specific cutting force for the given workpiece material.

Values of m_c and $k_{c1.1}$ can be found in the catalogs of cutting tool manufacturers and books. For 20MnCrS5 steel values are $m_c=0.25$ and $k_{c1.1}=2140 \text{ N}/\text{mm}^2$ [49]. The MAPE value of the main cutting force is about 60%, while for the experimental trials and for the validation test, it is about 65%. Steel S235JRG2 belongs to the universal workpiece material group, unalloyed and low-alloyed steels, $C > 0.55\%$, not tempered, according to cutting tool manufacturer Walter ($m_c=0.25$, $k_{c1.1}=1700 \text{ N}/\text{mm}^2$). The same values can be found in the Sandvik Coromant catalog [10]. For S235JRG2 steel values are $m_c=0.17$ and $k_{c1.1}=1780 \text{ N}/\text{mm}^2$ [49]. The MAPE value of the main cutting force for S235JRG2 steel is about 35%, while for the experimental trials and for the validation test, it is about 38%.

The exact values of coefficients m_c and $k_{c1.1}$ cannot be easily found because some materials may be thermally treated, while some specific materials have properties that are between the different workpiece materials subgroups offered in catalogs of cutting tool manufacturers or available databases.

However, the aforementioned Victor-Kienzle model gives approximate values of the main cutting force, which may be in poor agreement with the cutting force values obtained experimentally, while the main advantage is fast calculation.

4.3 Extended DA Model of the Main Cutting Force and Correction Coefficient for Tool Nose Radius

The cutting forces in the turning process are dependent not only on the properties of the workpiece material and cutting parameters, but also on the geometry of the cutting tool edge, which affects the chip shape (thickness and width). Tool nose radius is an important parameter that affects the cutting force. Parida et al. [50] analyzed the influence of tool nose radius on the main cutting force. Their study revealed that as tool nose radius increases, the main cutting force also increases due to the increased contact area. Increasing tool nose radius does not only increase the main cutting force, but also affects the components of the cutting force, i.e., causing an increase in the radial and a decrease in the axial force [51-53].

The extended main cutting force prediction models with a correction coefficient are given by Eqs. (11) and (12):

$$(20\text{MnCrS5}) F_c = 2.4865 \cdot 525 \cdot f^2 \cdot \left(\frac{v}{v_f}\right)^{0.09816} \cdot \left(\frac{a_p}{f}\right)^{0.89362} \cdot \left(\frac{\kappa}{\gamma_0}\right)^{0.01669} \cdot C_r \quad (11)$$

$$(S235JRG2) F_c = 1.4551 \cdot 540 \cdot f^2 \cdot \left(\frac{v}{v_f}\right)^{0.10746} \cdot \left(\frac{a_p}{f}\right)^{1.04605} \cdot \left(\frac{\kappa}{\gamma_0}\right)^{0.05254} \cdot C_r \quad (12)$$

where the correction coefficient was $C_r = 1$ in the case of using the tool nose radius of 0.8 mm or $C_r = 1.08$ in the case of using the tool nose radius of 1.2 mm.

In order to determine the correction coefficient (C_r), additional experimental trials were conducted for both steel materials using a cutting insert with a larger tool nose radius of 1.2 mm (Tables 9 and 10).

Table 9 Experimental trials for extended DA model of 20MnCrS5 steel

No.	v/v_f π_2	a_p/f π_3	κ/γ_0 π_4	F_c [N] experimentally	F_c [N] extended DA model
1	881.57	6.12	5.00	555	546.6
2	538.28	9.03	5.00	1972	1977.6
3	538.28	6.23	11.18	1300	1331.5

Table 10 Experimental trials for extended DA model of S235JRG2 steel

No.	v/v_f π_2	a_p/f π_3	κ/γ_0 π_4	F_c [N] experimentally	F_c [N] extended DA model
1	945.68	6.12	5.00	505	493
2	577.43	9.03	5.00	1882	1884.1
3	577.43	6.23	11.18	1226	1332.4

Increasing tool nose radius increased the main cutting force and its effect was consistent, given the same C_r value was obtained for both materials.

4.4 Analysis of Cutting Force Components

Based on the analysis of experimental results it was observed that for all three cutting force components, main cutting force (F_c), passive force, i.e., radial force (F_p), and feed force, i.e., axial force (F_f), the most important parameter was dimensionless group π_3 , i.e., chip slenderness ratio [43]. The cutting force components values obtained experimentally in laboratory conditions are shown in Tables 11 and 12 for 20MnCrS5 steel and S235JRG2 steel, respectively. The effect of the chip slenderness ratio on cutting force components is given in Fig. 7. For both workpiece materials, by increasing chip slenderness ratio, the main cutting force and feed force increase drastically, while the radial force decreases.

Table 11 Experimental design $3^3 \times 2^1$ of the cutting force components of 20MnCrS5 steel

No.	v/v_f π_2	a_p/f π_3	κ/γ_o π_4	F_c [N]	F_p [N]	F_f [N]
				experimentally		
1	693.93	7.63	5.00	969	172	478
2	693.93	7.63	11.18	977	197	497
3	881.57	6.12	5.00	508	144	247
4	881.57	9.18	11.18	742	155	404
5	538.28	9.03	5.00	1831	178	903
6	538.28	6.23	11.18	1334	282	634

Table 12 Experimental design $3^3 \times 2^1$ of the cutting force components of S235JRG2 steel

No.	v/v_f π_2	a_p/f π_3	κ/γ_o π_4	F_c [N]	F_p [N]	F_f [N]
				experimentally		
1	744.39	7.63	5.00	895	139	330
2	744.39	7.63	11.18	939	163	377
3	945.68	6.12	5.00	465	118	182
4	945.68	9.18	11.18	731	139	326
5	577.43	9.03	5.00	1747	181	712
6	577.43	6.23	11.18	1235	198	451

Analysis of the ratio of cutting force components provides useful insights into the efficiency and stability of the machining process. The ratio of the cutting force components F_c/F_f indicates the efficiency of material removal in relation to the side load of the cutting tool. A high value of this ratio is desirable because it indicates an efficient process with reduced side load, which can improve the quality of the machined surface and extend tool life. For both materials, it ranges from 1.8 to 2.7, which indicates more efficient cutting with less feed force. The ratio of the cutting force components F_c/F_p varies between 3.1 and 10.2, indicating that most of the energy is directed to the removal of material, potentially reducing wear and vibration. The ratio of the cutting force components F_f/F_p varies around 2, which indicates a stable process with reduced lateral load and vibrations, which can improve surface quality and extend tool life.

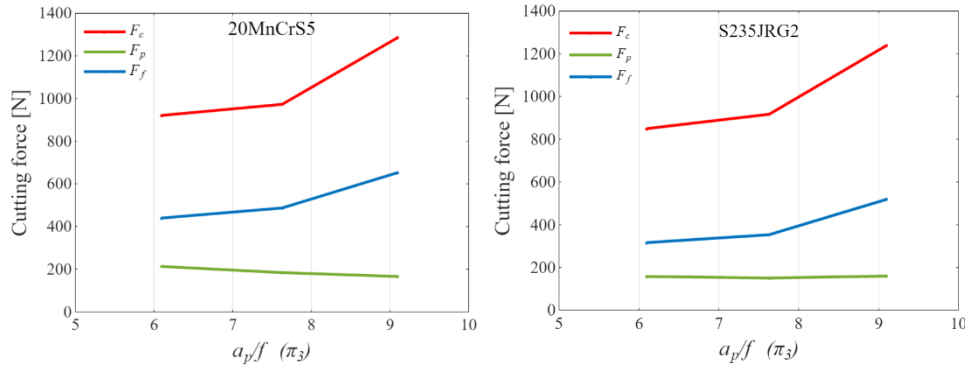


Fig. 7 The influence of the chip slenderness ratio (dimensionless group π_3) on the cutting force components

The ratios of the cutting force components for both steel materials (20MnCrS5 and S235JRG2) are analogous. The ratio of the cutting force components F_c/F_f decreases, while the ratios F_c/F_p and F_f/F_p increase with an increase in the chip slenderness ratio.

It is not possible to predict all cutting force components using only one extended DA model, considering that the ratios of the cutting force components change.

5. CONCLUSION

This study proposed a novel approach to predicting the cutting force in turning using dimensional analysis. Experimental investigation in dry longitudinal single-pass turning of two steel materials, 20MnCrS5 steel and S235JRG2 steel, was considered using Taguchi's $3^3 \times 2^1$ design with additional validation trials. Based on the conducted analyses, experimental and modeling results, the following conclusions may be drawn:

- The proposed models derived using DA and limited experimental data proved to be able to accurately predict the main cutting force.
- Additional validation tests with parameter values outside the initial experimental hyper-space showed very good extrapolation capabilities of the proposed models for predicting the main cutting force.
- Chip slenderness ratio was the most important parameter affecting the main cutting force, followed by the ratio of cutting speed and feed velocity, while the effect of the ratio of the cutting edge angle and rake angle was the least pronounced.
- The well-known Victor-Kienzle model can be used to predict the cutting force if the exact values of m_c and $k_{c1.1}$ coefficients are known for the particular material used in the cutting process.
- The derived extended main cutting force prediction models showed a consistent positive correlation between tool nose radius and the main cutting force.
- The proposed models proved to be valid for predicting all three cutting force components with high accuracy. It was found that by increasing the chip slenderness ratio, the main cutting force and feed force increased drastically, while the radial force decreased. In this regard, the ratios F_c/F_p and F_f/F_p are subject to change,

considering the selected values of a_p and f (or chip slenderness ratio), while the ratio F_c/F_f is approximately constant.

It can be concluded that DA-based models have a very good potential for reliable and accurate estimation of the cutting force in turning. The discussed approach can take into account a large number of cutting parameters using a smaller number of experimental trials, which plays a significant role not only regarding prediction performance but also in great economy, reduced experimentation time, and saving materials and energy for conducting experiments. The limitation of the proposed DA-based models is that it would be necessary to extend these models in case of significant parameter interactions. In addition, the existence of multiple dimensionless groups with a number of parameters makes it difficult to define levels of variation and selection of appropriate experimental designs.

In order to derive the greatest benefit from the calculations and experimental methods used in the present work, it is also necessary to open the door to new possibilities of DA modeling, i.e., the application of the DA model for determining the model of surface roughness, cutting temperature, etc.

Future research will probably be in the direction of determining the correction coefficients of the cutting parameters and predicting other performances based on the cutting force assessment (power consumption, cutting temperature, tool wear, friction, etc.).

Acknowledgement: *This research was financially supported by the Ministry of Science, Technological Development and Innovation of the Republic of Serbia (Contract No. 451-03-65/2024-03/200109 and 451-03-65/2024-03/200155).*

REFERENCES

1. He, C.L., Zong, W.J., Zhang, J.J., 2018, *Influencing factors and theoretical modeling methods of surface roughness in turning process: state-of-the-art*, International Journal of Machine Tools and Manufacture, 129, pp. 15-26.
2. Madić, M., Trifunović, M., Janković, T., 2022, *Development and analysis of surface roughness model in dry straight turning of C45E steel*, Innovative Mechanical Engineering, 1(2), pp. 11-21.
3. Madić, M., Girdu, C., Marinković, D., Janković, P., Trifunović, M., 2024, *Analysis of kerf width and its variation in CO2 laser cutting of straight and curved cut profiles*, Tehnicki Vjesnik, 31(6), pp. 1884-1891.
4. Nag, A., Dixit, A.R., Petru, J., Vaňová, P., Konečná, K., Hloch, S., 2024, *Maximization of wear rates through effective configuration of standoff distance and hydraulic parameters in ultrasonic pulsating waterjet*, Facta Universitatis-Series Mechanical Engineering, 22(2), pp. 165-186.
5. Madić, M., Petrović, G., Petković, D., Janković, P., 2024, *Traditional and integrated MCDM approaches for assessment and ranking of laser cutting conditions*, Spectrum of Mechanical Engineering and Operational Research, 1(1), pp. 250-257.
6. Wang, S., Tao, Z., Wenping, D., Zhanwen, S., To, S.S., 2022, *Analytical modeling and prediction of cutting forces in orthogonal turning: a review*, The International Journal of Advanced Manufacturing Technology, 119(3-4), pp. 1407-1434.
7. Rytir, M., Rönnecke, J., Hänel, A., Kolar, P., Ihlenfeldt, S., 2023, *Influence of engagement parameters on estimation of tangential cutting force using high-frequency process data of the machine tool*, Procedia CIRP, 118(1), pp. 537-542.
8. Zhang, G., Guo, C., 2015, *Modeling of cutting force distribution on tool edge in turning process*, Procedia Manufacturing, 1, pp. 454-465.
9. Sousa, V.F., Silva, F.J., Fecheira, J., Lopes, H.M., Martinho, R.P., Casais, R.B., Ferreira, L.P., 2020, *Cutting forces assessment in CNC machining processes: a critical review*, Sensors, 20(16), 4536.
10. Zeman, P., Kovalčík, J., Vrabec, M., 2014, *Principles of cutting process modelling and new algorithm proposal*, Manufacturing Technology, 14(4), pp. 658-664.

11. Hanief, M., Wani, M.F., Charoo, M.S., 2017, *Modeling and prediction of cutting forces during the turning of red brass (C23000) using ANN and regression analysis*, Engineering Science and Technology, an International Journal, 20(3), pp. 1220-1226.
12. Ma, L., Li, C., Chen, J., Li, W., Tan, Y., Wang, C., Zhou, Y., 2017, *Prediction model and simulation of cutting force in turning hard-brittle materials*, The International Journal of Advanced Manufacturing Technology, 91(1-4), pp. 165-174.
13. Korkmaz, M.E., Yasara, N., Günay, M., 2020, *Numerical and experimental investigation of cutting forces in turning of Nimonic 80A superalloy*, Engineering Science and Technology, an International Journal, 23(3), pp. 664-673.
14. Lukács, J., Horváth, R., 2022, *Comprehensive investigations of cutting with round insert: introduction of a predictive force model with verification*, Metals, 12(2), 257.
15. Suresh, R., Basavarajappa, S., Samuel, G. L., 2012, *Some studies on hard turning of AISI 4340 steel using multilayer coated carbide tool*, Measurement, 45(7), pp. 1872-1884.
16. Bouzid, L., Yaltese, M.A., Belhadi, S., Haddad, A., 2020, *Modelling and optimization of machining parameters during hardened steel AISID3 turning using RSM, ANN and DFA techniques: comparative study*, Journal of Mechanical Engineering and Sciences, 14(2), pp. 6835-6847.
17. Ozdemir, M., Ercan, K., Buyuker, B., Akyildiz, H.K., 2021, *Analysis of the effect of tool nose radius, feed rate, and cutting depth parameters on surface roughness and cutting force in CNC lathe machining of 36CrNiMo4 alloy steel*, Journal of Science, Part A: Engineering and Innovation, 8(2), pp. 308-317.
18. Hamdi, A., Yaltese, M.A., Chaoui, K., Mabrouki, T., Rigal, J.F., 2012, *Analysis of surface roughness and cutting force components in hard turning with CBN tool: prediction model and cutting conditions optimization*, Measurement, 45(3), pp. 344-353.
19. Meddour, I., Yaltese, M.A., Bensouilah, H., Khellaf, A., Elbah, M., 2018, *Prediction of surface roughness and cutting forces using RSM, ANN, and NSGA-II in finish turning of AISI 4140 hardened steel with mixed ceramic tool*, The International Journal of Advanced Manufacturing Technology, 97(5-8), pp. 1931-1949.
20. Tang, L., Cheng, Z., Huang, J., Gao, C., Chang, W., 2015, *Empirical models for cutting forces in finish dry hard turning of hardened tool steel at different hardness levels*, The International Journal of Advanced Manufacturing Technology, 76(1-4), pp. 691-703.
21. Ibraheem, M.Q., 2020, *Prediction of cutting force in turning process by using Artificial Neural Network*, Al-Khwarizmi Engineering Journal, 16(2), pp. 34-46.
22. Alajmi, M.S., Almeshal, A.M., 2021, *Modeling of cutting force in the turning of AISI 4340 using Gaussian Process Regression Algorithm*, Applied Sciences, 11(9), 4055.
23. Safi, K., Yaltese, M.A., Belhadi, S., Mabrouki, T., Chihaoui, S., 2023, *Modeling of cutting force and power consumption using ANN and RSM methods in turning of AISI D3 comparative study and precision benefit*, Journal of Theoretical and Applied Mechanics, 53(1), pp. 49-65.
24. Toubhans, B., Fromentin, G., Viprey, F., Karaoui, H., Dorlin, T., 2020, *Machinability of Inconel 718 during turning: Cutting force model considering tool wear, influence on surface integrity*, Journal of Materials Processing Technology, 285, 116809.
25. Nur, R., Yusof, N.M., Izman, S., Nor, F.M., Kurniawan, D., 2021, *Determination of energy consumption during turning of hardened stainless steel using resultant cutting force*, Metals, 11(4), pp. 565.
26. Krupa, V., Tymoshenko, N., Kobelnyk, V., Petrechko, I., 2022, *Probability-statistical estimation method of feed influence on the tangential cutting force under turning*, Journal of Achievements in Materials and Manufacturing Engineering, 114(1), pp. 22-31.
27. Fodor, G., Sykora, H.T., Bachrathy, D., 2020, *Stochastic modeling of the cutting force in turning processes*, The International Journal of Advanced Manufacturing Technology, 111(1-2), pp. 213-226.
28. Abdellaoui, L., Khlifi, H., Bouzid Sai, W., Hamdi, H., 2021, *Tool nose radius effects in turning process*, Machining Science and Technology, 25(1), pp. 1-30.
29. Horváth, R., 2015, *A new model for fine turning forces*, Acta Polytechnica Hungarica, 12(7), pp. 109-128.
30. Zakrzewski, T., Kozak, J., Witt, M., Debowska-Wasak, M., 2020, *Dimensional Analysis of the effect of SLM parameters on surface roughness and material destiny*, Procedia CIRP, 95(4), pp. 115-120.
31. Bazaz, S.M., Ratava, J., Lohtander, M., Varis, J., 2023, *An investigation of factors influencing tool life in the metal cutting turning process by dimensional analysis*, Machines, 11(3), 393.
32. Mahoneya, J., Yeralan, S., 2019, *Dimensional Analysis*, Procedia Manufacturing, 38(1), pp. 694-701.
33. Nain, G.M., Hipparagi, M.A., Bellubbi, S., Roy, A., Anjan, B.N., Ramesh, S., Narendranath, S., 2022, *A study on dimensional analysis modeling of crater size during wire electrical discharge turning process by using Buckingham Pi theorem*, Materials today, 66(4), pp. 2093-2097.
34. Adiutori, E., 2018, *An alternate view of dimensional homogeneity*, The Open Mechanical Engineering Journal, 12(1), pp.164-174.

35. Bolboaca, S.D., Jantschi, L., 2007, *Design of experiments: useful orthogonal arrays for number of experiments from 4 to 16*, Entropy, 9(4), pp. 198-232.
36. Stephenson, D.A., Agapiou, J.S., 2018, *Metal cutting theory and practice*, CRC press, 3rd Edition, Boca Raton, London, 947 p.
37. Chuangwen, X., Jianming, D., Yuzhen, C., Huaiyuan, L., Zhicheng, S., Jing, X., 2018, *The relationships between cutting parameters, tool wear, cutting force and vibration*, Advances in Mechanical Engineering, 10(1), pp. 1-14.
38. Magdum, V.B., Naik, V.R., 2017, *Investigating feed rate effect on cutting force of EN 8 turning*, Asian Review of Mechanical Engineering, 6(1), pp. 8-12.
39. Demir, Z., Adiyaman, O., 2018, *A mathematical approach to investigate the effect of chip slenderness ratio in primary deformation zone in turning*, Academia Journal of Scientific Research, 6(9), pp. 351-357.
40. Denkena, B., Breidenstein, B., Kroedel, A., Prasanthan, V., 2021, *Chip formation in machining hybrid components of SAE1020 and SAE5140*, Production Engineering, 15(1), pp. 187-197.
41. Vedashree, K.N., Shailesh, R., 2020, *A Study on the effect of rake Angle and depth of cut on cutting forces during orthogonal cutting*, International Journal of Innovative Research in Science, Engineering and Technology, 9(5), pp. 3175-3179.
42. Vipran, B., Palwinder, S., Rishi, S., 2018, *Effect of cutting parameters on cutting force under different conditions in hard turning of AISI4340*, Research Journal of Engineering and Technology, 9(1), pp. 45-54.
43. Demir, Z., Adiyaman, O., 2019, *Investigation of influence of approach angle and chip slenderness ratio on vibration, chip formation and surface quality in turning of AISI 1050 steel*, Journal of the Brazilian Society of Mechanical Sciences and Engineering, 41, 467.
44. Grigoriev, S.N., Fedorov, S.V., Hamdy, K., 2019, *Materials, properties, manufacturing methods and cutting performance of innovative ceramic cutting tools a review*, Manufacturing Review, 6(19), pp. 1-27.
45. Yilmaza, B., Karabulut, S., Güllüa, A., 2020, *A review of the chip breaking methods for continuous chips in turning*, Journal of Manufacturing Processes, 49, pp. 50-69.
46. Denkena, B., Kroedel, A., Ellersiek, L., Zender, F., 2021, *Modeling of process force for complex multi axial turning processes*, MM Science Journal, 5, pp. 5023-5029.
47. Karpuschewski, B., Kunderák, J., Varga, G., Deszpoth, I., Borysenko, D., 2018, *Determination of specific cutting force components and exponents when applying high feed rates*, Procedia CIRP, 77(9), pp. 30-33.
48. Augspurger, T., Schraknepper, D., Bergs, T., 2020, *Experimental investigation of specific cutting forces and estimation of the heat partitioning under increasing tool wear in machining nickel based super alloy IN718*, Production Engineering, 14(1-3), pp. 491-498.
49. <https://mac.walter-tools.com> (last access: 10.11.2024.)
50. Parida, A.K., Maity, K., 2017, *Effect of nose radius on forces, and process parameters in hot machining of inconel 718 using finite element analysis*, Engineering Science and Technology, an International Journal, 20(2), pp. 687-693.
51. Li, W., Zhou, B., Xing, L., He, H., Ni, X., Li, M., Gong, Z., 2023, *Influence of cutting parameters and tool nose radius on the wear behavior of coated carbide tool when turning austenitic stainless steel*, Materials Today Communications, 37, 107349.
52. Balwan, V.R., Dabade, B., Wankhade, L., 2022, *Influence of hard turning parameters on cutting forces of EN 353 steel*, Materials Today, 63(1), pp. 149-156.
53. Rao, A.S., 2023, *Effect of nose radius on the chip morphology, cutting force and tool wear during dry turning of Inconel 718*, Tribology-Materials, Surfaces & Interfaces, 17(1), pp. 62-71.